AD-A062 240 ENVIRONMENTAL RESEARCH AND TECHNOLOGY INC CONCORD MASS F/G 4/2
THIN CIRRUS CLOUD OVER THE TROPICAL PACIFIC,(U)
OCT 78 H K BURKE, A J BUSSEY, K R HARDY F19628-76-C-0069
UNCLASSIFIED ERT-P-1996-637F AFGL-TR-78-0259 NL

1 OF 1
AD A062240

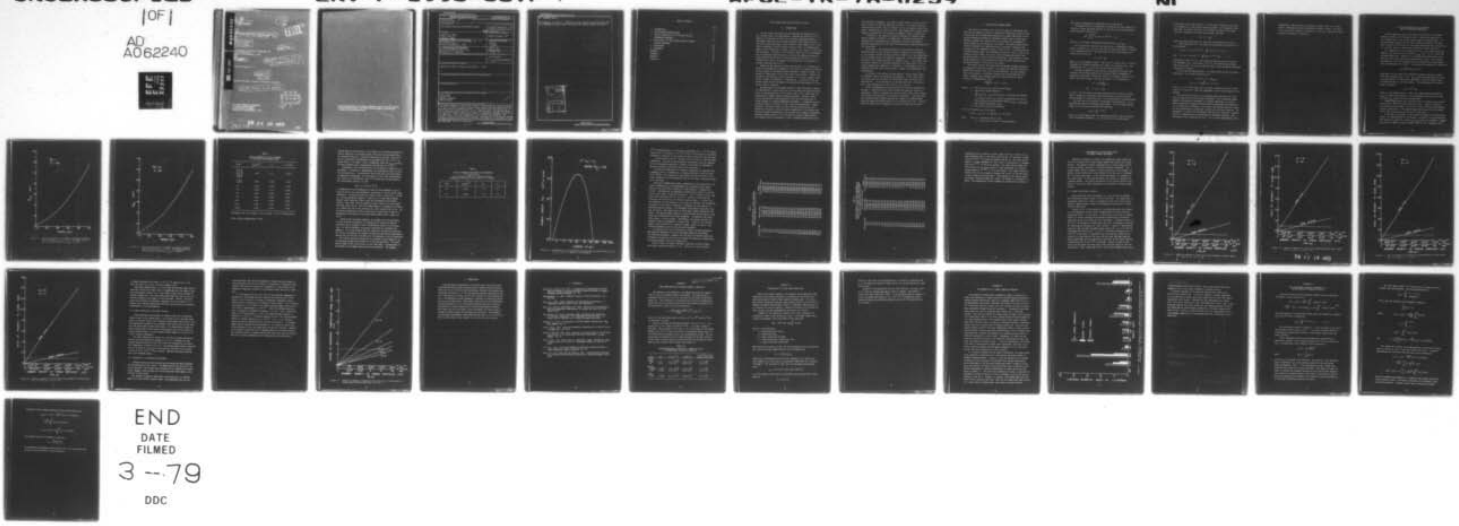

END
DATE FILMED
3-79
DDC

(13) (19) AFGL-TR-78-0259

(12) LEVEL II

(6) THIN CIRRUS CLOUD OVER THE TROPICAL PACIFIC

(10) Hsiao-hua K./Burke,
Allan J./Bussey
Kenneth R./Hardy

(12) 41p.

Environmental Research & Technology, Inc.
696 Virginia Road
Concord, Massachusetts 01742

(11) Oct 78

(14) ERT-P-1996-637F
SCIENTIFIC-3

Scientific Report No. 3

(16) 627A

(17) 00

Approved for public release; distribution unlimited

(15) F19628-76-C-0069

AIR FORCE GEOPHYSICS LABORATORY
AIR FORCE SYSTEMS COMMAND
UNITED STATES AIR FORCE
HANSCOM AFB, MASSACHUSETTS 01731

Unclassified

SECURITY CLASSIFICATION OF THIS PAGE *(When Data Entered)*

REPORT DOCUMENTATION PAGE

READ INSTRUCTIONS BEFORE COMPLETING FORM

1. REPORT NUMBER: AFGL-TR-78-0259	2. GOVT ACCESSION NO
3. RECIPIENT'S CATALOG NUMBER	
4. TITLE *(and Subtitle)*: Thin Cirrus Cloud over the Tropical Pacific	5. TYPE OF REPORT & PERIOD COVERED: Scientific Report No. 3
6. PERFORMING ORG. REPORT NUMBER: ERT-P-1996-637F	
7. AUTHOR(s): Hsiao-hua K. Burke Allan J. Bussey Kenneth R. Hardy	8. CONTRACT OR GRANT NUMBER(s): F19628-76-C-0069
9. PERFORMING ORGANIZATION NAME AND ADDRESS: Environmental Research & Technology, Inc. 696 Virginia Road Concord, Massachusetts 01742	10. PROGRAM ELEMENT, PROJECT, TASK AREA & WORK UNIT NUMBERS: 62101F 627A00BE
11. CONTROLLING OFFICE NAME AND ADDRESS: Air Force Geophysics Laboratory Hanscom AFB, Massachusetts 01731 Monitor/Peter A. Giorgio/LY	12. REPORT DATE: October 1978 13. NUMBER OF PAGES: 39
14. MONITORING AGENCY NAME & ADDRESS *(if different from Controlling Office)*	15. SECURITY CLASS. *(of this report)*: Unclassified 15a. DECLASSIFICATION/DOWNGRADING SCHEDULE

16. DISTRIBUTION STATEMENT *(of this Report)*

Approved for public release; distribution unlimited

17. DISTRIBUTION STATEMENT *(of the abstract entered in Block 20, if different from Report)*

18. SUPPLEMENTARY NOTES

19. KEY WORDS *(Continue on reverse side if necessary and identify by block number)*

cirrus cloud
severe-clear
radiative transfer
remote sensing

micrometers

20. ABSTRACT *(Continue on reverse side if necessary and identify by block number)*

This report summarizes a theoretical study of the detectability of high altitude (>10 km) thin cirrus clouds by various remote sensors over the tropical Pacific. The remote sensors considered include (1) visual detection from the surface, (2) visual detection from an aircraft, and (3) infrared sensor (6.7 μm) from space. The radiative transfer technique to compute the atmospheric radiance (intensity) is summarized. The optical properties of ice crystals are presented. The results indicate that the minimum detectable concentration of ice crystals having a dimension greater than 80 μm, the critical size which will be hazardous to the

DD FORM 1 JAN 73 1473 EDITION OF 1 NOV 65 IS OBSOLETE

micrometers

Unclassified

SECURITY CLASSIFICATION OF THIS PAGE *(When Data Entered)*

20. ABSTRACT (cont)

RV transition, is around 2 x 10^{4} m^{-3} for visual detection from the surface and 3-4 x 10^{3} m^{-3} for both aircraft observation and infrared sensors from space.

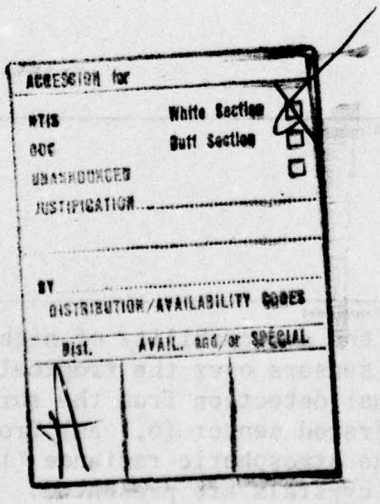

TABLE OF CONTENTS

THIN CIRRUS CLOUD OVER THE TROPICAL PACIFIC

1. INTRODUCTION

In this study, the problem of the existence of tenuous cirrus in the tropical Pacific has been pursued. Defining the existence and probability of occurrence of thin cirrus clouds is important because of the requirement that there be a natural transition from laminar to turbulent flow over reentering objects, which normally occurs around 10 km. Microscopic roughening of the RV surface caused by impact of isolated hydrometeors can be sufficient to trigger transition and thereby to invalidate the experiment. According to one estimate, there will be an intolerable risk of premature transition above a 10 km height whenever particles larger than 80 microns occur in concentrations of more than 1 m^{-3}. A "severe-clear" case or the absence of any detectable ice particles is therefore required above 10 km.

Because of the sparcity of direct measurements, it is difficult to define the atmospheric environment in the vicinity of reentering vehicles for the purpose of evaluating natural atmospheric effects on them. The attempt of identifying cirrus clouds along reentry paths is further complicated by the multiple of their possible crystal sizes, shapes, orientations, numbers and densities. Consequently, a sensitivity study of various remote sensing techniques for quantitative measurements of thin cirrus clouds is required.

The advantage of using remote sensors is that they provide continuous information on cirrus properties in the vicinity of actual reentries. Using in situ measurements in the reentry area, on the other hand, can cause possible dangers from the reentering object. However, remote sensors provide only certain quantities that are often difficult to relate uniquely to standard atmospheric parameters. Assumptions have to be made in order to retrieve all the cirrus cloud quantities: height, thickness, ice water content, crystal size and concentrations, etc. Theoretical estimates, based on optical properties of ice crystals and radiative transfer computations, are carried out to predict the minimum detectable number density of ice crystals for various remote sensors. The standard tropical atmosphere is used as ambient conditions to simu-

late Kwajalein atmosphere. The various remote sensors discussed in this report include (1) eyeball detection at surface, (2) eyeball detection from aircraft altitude, and (3) infrared (6.7 μm wavelength) sensor from space. Capabilities of radar and lidar some common active sensors being operated at Kwajalein, are presented in Appendix A and B, respectively.

In Section 2, the radiative transfer technique to calculate atmospheric radiance (intensity) is summarized. The method includes the contribution of absorption due to atmospheric gaseous constituents, multiple scattering due to both the cloud particles and molecules, and surface reflection.

In Section 3, the optical properties of ice crystals, which are essential input for the radiative transfer computation, are presented. In this section, results of long circular cylinders are used; computations for ice spheres are also included for comparison. Since the sphere computation is far simpler and uses less computer time, it may be that some correlation factor can be defined between an ice sphere and cylinder to reduce computational complexity. Furthermore, a Deirmendjian size distribution function (1964) is presented to compare with monodisperse size distribution.

In Section 4, the results of detectability of thin cirrus layers of different sensors are presented and compared. In the visible spectral range, both the sun angle and observation angle can affect the detectability. At IR wavelength, the antenna angle plays an important role. Such dependences are also shown in this section.

Future recommendations for detecting thin cirrus are presented in Section 5. Observations both from aircraft and satellite sensors are considered. Finally, a probability study of severe-clear versus tenuous cirrus cases over Kwajalein is presented in Appendix C. Available data sets include surface weather observations, upper air soundings, DMSP satellite images and RAOB reports over the calendar year 1975. Optimum months of the year for scheduling a severe-clear shot are discussed.

2. THE RADIATIVE TRANSFER MODEL

The radiative transfer model provides a means of theoretical estimates of the radiance (intensity) received at either the surface or from aircraft due to the downwelling radiation or a space vehicle due to the upwelling radiation through an atmosphere either clear or with clouds. Radiance estimates are calculations of the amount of electromagnetic energy emitted at the frequencies considered. The total energy received (sensed) represents the combined effects of emission, absorption and scattering of the atmosphere within a field of view. In the visible and infrared spectral range, the atmospheric absorption effect is due to the presence of water vapor, mixed gas, ozone, nitrogen and aerosol; the scattering effect is both aerosol and molecular. The presence of clouds further complicates the problem due to their discrete scattering and absorption properties within the cloud layers.

The formal relation which describes the passage through a medium is the equation of radiative transfer. It governs the radiation field in a medium which absorbs, emits and scatters radiation. The most general form of the equation of radiative transfer for a plane-parallel atmosphere, assuming axial symmetry about the zenith direction, can be written as (Chandrasekhar, 1960):

$$\mu \frac{dI(\tau,\mu)}{d\tau} = I(\tau,\mu) - J(\tau,\mu)$$

where μ = the cosine of the vertical zenith angle,

τ = the optical depth defined as $\int_{\infty}^{z} \gamma_{ext}(z)dz$, γ_{ext} being the total extinction coefficient at altitude z above the surface, representing the sum of both scattering and absorption effects ($\gamma_{ext} = \gamma_{scat} + \gamma_{abs}$)

I = the radiance (intensity), and

J = the source function of radiation.

The source function can be written as

$$J(\tau,\mu) = J_o(\tau,\mu) + 1/2 \int_{-1}^{1} p(\mu,\mu') \, I(\tau,\mu')d\mu'$$

where $p(\mu,\mu')$ = the phase function, and

J_o = the primary excitation source function.

The explicit dependence on wavelength has been suppressed.

The phase function is normalized to represent the total energy scattered by a single scatterer relative to the sum of the energy absorbed and scattered by the particle:

$$\frac{1}{4\pi} \int_{-1}^{1} \int_{0}^{2\pi} p(\mu,\phi;\mu',\phi')d\mu'd\phi' = \omega_o \leq 1$$

where ω_o is the single scattering albedo defined as $\gamma_{sca}/\gamma_{ext}$.

For an isotropic scatterer, the scattering is independent of angle and p = constant = ω_o. For ice crystals, the scattering effect is largely in the forward direction. The phase function for an anisotropic scatterer can be written as

$$p = \omega_o(1 + 3g)$$

where g is the assymmetry factor. The value of g varies from -1 (totally backward) to 1 (totally forward) with 0 being the isotropic case. The determination of ω_o, g and τ will be presented in Section 3.

In order to simplify the anisotropic scattering, similarity transformation relationships given by van de Hulst (1967) are adopted to approximate anisotropic scattering. Given the assymmetry factor g, the single scattering albedo ω' and optical depth τ' are transformed to

$$\omega_o' = \left(\frac{1 - g}{1 - \omega_o g}\right) \omega_o$$

and $$\tau' = \tau(1 - \omega_o g)$$

ω_o' and τ' are the single scattering albedo and optical depth one would have to assume in an isotropic scattering problem in order to obtain results similar to those for ω_o and τ in the anisotropic scattering medium.

The term yet to be defined is the primary source function. It is a function that varies for different wavelengths. In the visible spectral range, it is the solar radiation field such that

$$J_o(\tau) = \frac{p}{4} F e^{-\tau/\mu_o}$$

where πF is the primary solar flux reaching the earth's upper atmosphere at the wavelength considered, μ_o is the cosine of the solar zenith

angle and p is the phase function. In the case of isotropic scattering, p is reduced to ω_o, the single scattering albedo. In the thermal infrared range, the source function can be written in terms of the Planck function, assuming local thermal equilibrium, such that

$$J_o = (1 - \omega_o)B$$

where the Planck function B is a function of wavelength and temperature.

After solving for $J(\tau)$, the upwelling and downwelling radiances can be written as:

$$I(\tau,\mu) = I(\tau^*,\mu)e^{-(\tau^*-\tau)/\mu} + \int_{\tau}^{\tau^*} J(t)e^{-(t-\tau)/\mu}\, dt/\mu$$

and $$I(\tau,-\mu) = I(o,-\mu)e^{-\tau/\mu} + \int_{o}^{\tau} J(t)e^{-(\tau-t)/\mu}\, dt/\mu \qquad (\mu > 0)$$

respectively, where $I(\tau^*,\mu)$ = the upwelling radiance from the bottom of the atmosphere (i.e., the surface), $I(0,-\mu)$ = the downwelling radiance from the top and τ^* is the total optical depth of the atmosphere considered (from space to surface).

$I(\tau^*,\mu)$ has two contributions: (1) surface emission and (2) surface reflection. For a surface reflectivity R

$$I_1(\tau^*,\mu) = (1 - R)B_{surf}$$

$$I_2(\tau^*,\mu) = 2 \cdot R \cdot \int_o^1 I(\tau^*,-\mu')\mu' d\mu'$$

where $I_1 = 0$ in visible range and I_2 assumes a Lambertian surface; there will be an "isotropic" reflection independent of the incident angle on the surface.

The variational-iterative (VI) approach (Burke and Sze, 1977; Sze, 1976) is used to solve this system of equations. The variational method depends on finding the "extremum" of a certain functional; an a priori form is used for the unknown function and the coefficients are found from a set of minimizing conditions. In essence, this method provides a direct way for constructing an approximate solution for the source function. The atmosphere is divided into subintervals and the source function is approximated as a combination of step functions in different intervals. The advantages of this technique are that: (1) it is fast and requires little

computational time to achieve satisfactory accuracy, and (2) it allows vertical inhomogeneity and the inclusion of surface effects. The detail of the variational-iterative technique for solving the radiative transfer equation is presented in Appendix D.

3. OPTICAL PROPERTIES OF ICE CRYSTALS AND THE BACKGROUND ATMOSPHERE

Cirrus clouds are usually considered to consist of ice cylinders randomly oriented in the horizontal plane. The optical properties of ice cylinders both in the visible and IR regions are poorly known. Very few experimental results are available; moreover, because of the great deal of analytic difficulties in scattering computations for non-spherical ice crystals, there are insufficient theoretical results available.

The computations of the assymmetry factor g, the single scattering albedo ω_o and the extinction coefficient γ_{ext} (km^{-1}) in the visible and infrared regions for a sample of ice cylinders have been carried out by Roewe and Liou (1978, and private communication, 1978). The cylinders considered are 200 μm in length and 30 μm in radius with a mean monodisperse concentration of 0.05 cm^{-3}. The extinction coefficient is defined as

$$\gamma_{ext} = \int_o^\infty \pi N(r)\ Q_{ext}\ r^2\ dr$$

where N(r) dr is the drop size distribution function (per unit volume with radii between r and r + dr). Q_{ext} is the Mie efficiency factor for extinction which is a function of wavelength, radius and complex index of refraction and r is the drop radius. For a monodisperse size distribution it becomes

$$\gamma_{ext} = \pi r^2 n\ Q_{ext}$$

where n is the number density. Thus, for a monodisperse distribution, γ_{ext} is linearly proportional to the concentration such that it is easy to obtain γ_{ext} values for other concentrations.

Similar computations were carried out for ice spheres using the Mie theory (Dave, 1968; Gaut and Reifenstein, 1969). Figures 3-1 and 3-2 are results for wavelength 0.7 μm and 6.7 μm in the visible and infrared regions, respectively. The spheres range from 10 μm to 60 μm in radius with a mean concentration of 0.05 cm^{-3} in each case.

A 200 μm/30 μm cylinder is equivalent (in volume) to a 50 μm radius sphere. By comparing Table 1 and Figures 3-1 and 3-2, it is noticed that the values of ω_o and g are similar but β_{ext} (km^{-1}) for cylinders is higher than that for spheres of equal volume by 50% to 150%. Therefore, for a

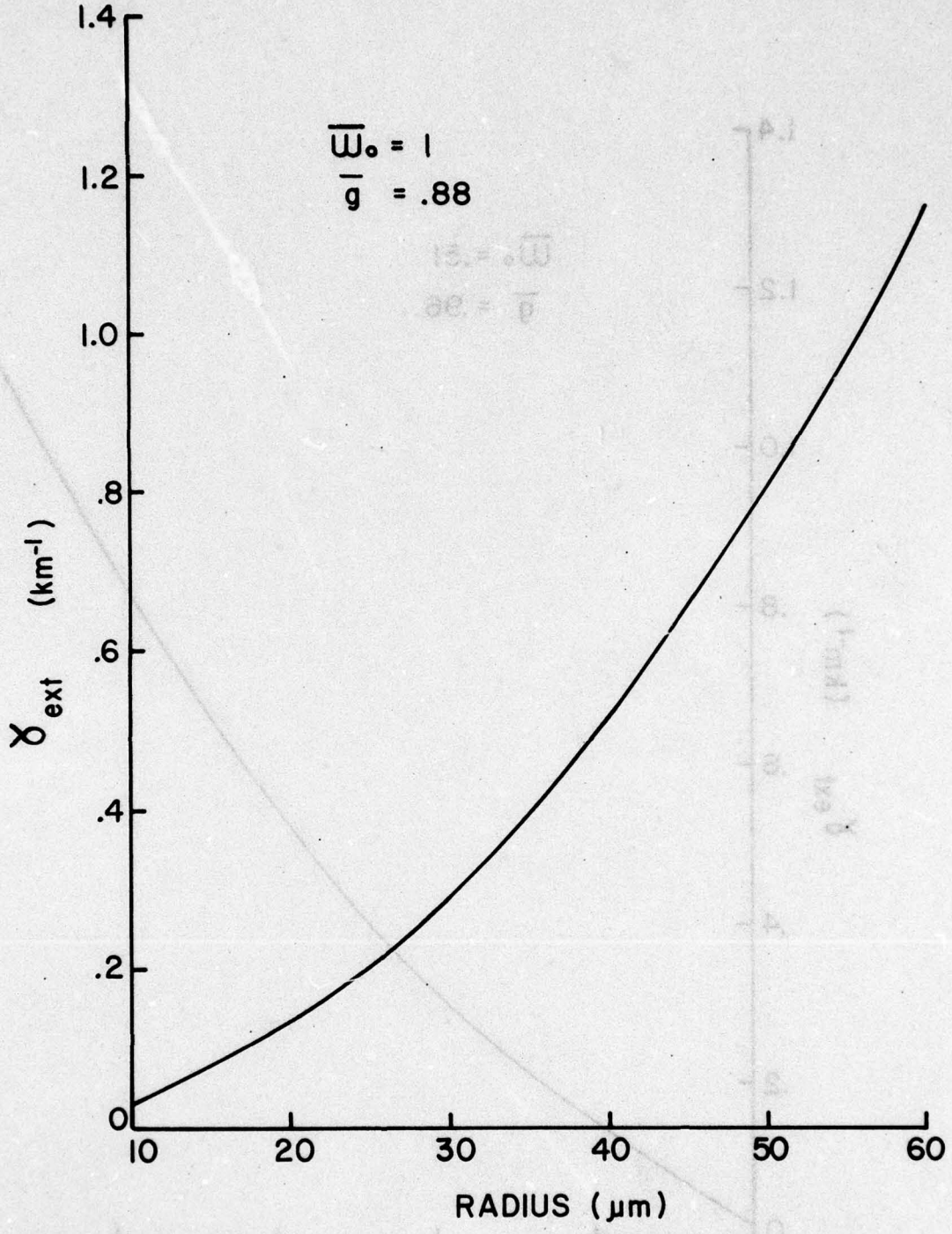

Figure 3-1 Optical properties of ice spheres assuming a concentration of 0.05 cm^{-3} at λ = 0.7 μm. For radius of 50 μm, the extinction coefficient (γ_{ext}) is 8 km^{-1}.

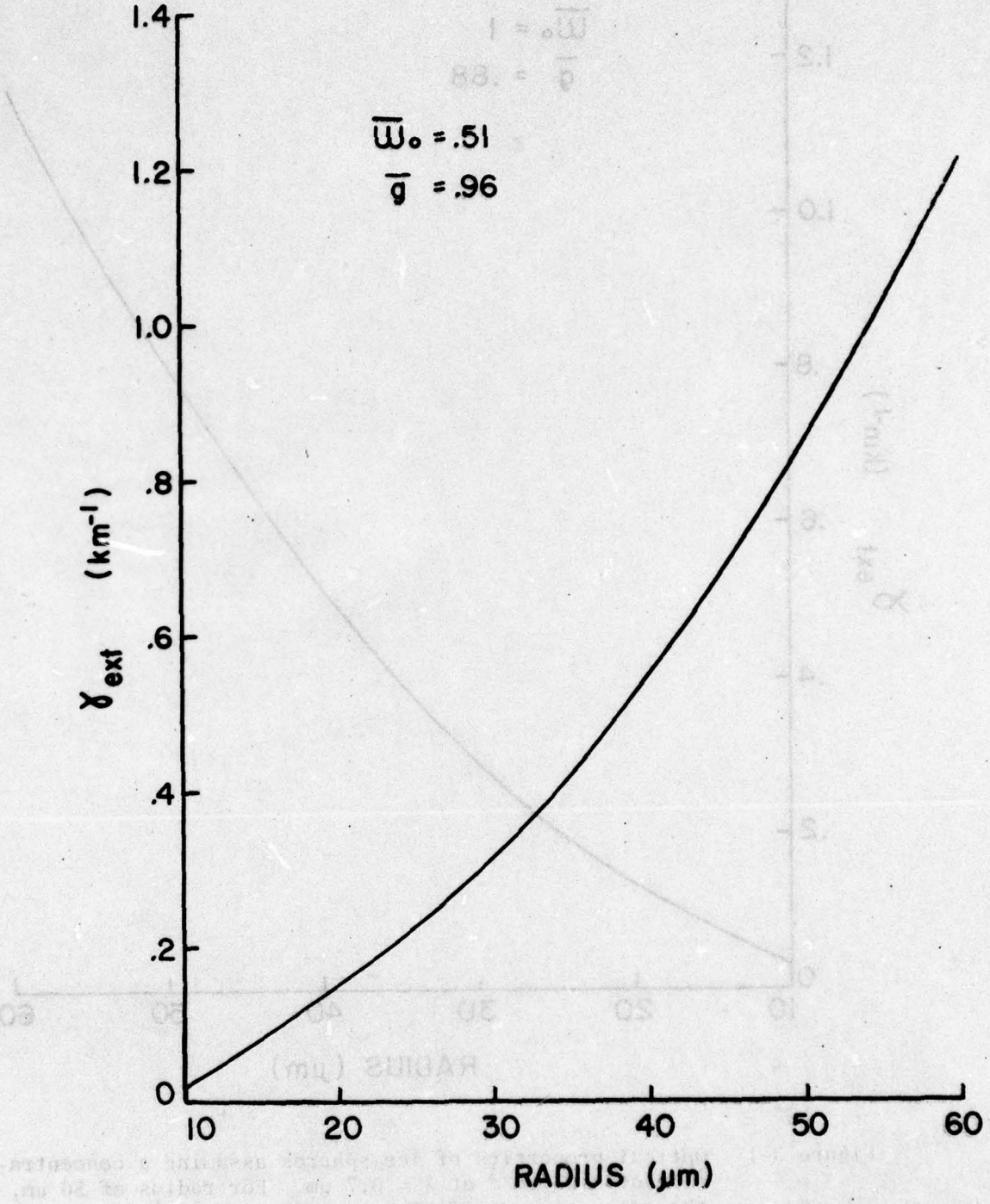

Figure 3-2 Optical properties of ice spheres assuming a concentration of 0.05 cm^{-3} at λ = 6.7 μm. For radius of 50 μm, the extinction coefficient (γ_{ext}) is 0.85 km^{-1}.

TABLE 1

OPTICAL PROPERTIES OF ICE CYLINDERS
IN THE SOLAR AND INFRARED BANDS*

λ(μm)	$\gamma_{ext}(km^{-1})$	ω_o	g = <cosΘ>
0.3 0.5 0.7 0.94 1.10	1.141	1.0	0.799
1.38 1.87	1.280	0.783	0.750
2.7	1.357	0.901	0.753
3.2	1.259	0.[illegible]24	0.651
4.3	1.416	0.542	0.675
6.3	2.082	0.511	0.791
10.0	1.437	0.531	0.857
15.0	1.467	0.527	0.671
18.69	1.556	0.554	0.729

*Cylinders, 200 μm in length, 30 μm in radius, 0.05 cm^{-3} concentration.

(Liou, private communication, 1978)

defined mass of ice particles, the cylinders will certainly dominate the optical properties to a greater extent than would the equivalent mass for spherical particles. Using the same kind of scaling, a new set of optical properties is defined for ice cylinders with size of 100 μ in length and 10 μ is radius. Table 2 summarizes values of γ_{ext}, ω_o and g of these cylinders with a monodisperse distribution of .05 cm^{-3}.

Furthermore, the size distribution of ice particles should also be considered. In reality, a monodisperse size distribution does not exist for cloud particles. The particular form of the drop size distribution is empirically determined. For the purpose of this study the Deirmendjian (1964) size distribution, which is the most general specification for cloud droplet spectra, is used:

$$N(r) = A\, r^{C_1} \exp\{-B\, r^{C_2}\}$$

It characterizes the distribution in terms of four parameters; two of which (A and B) are scale parameters, the others (C_1 and C_2) being shape parameters. For high altitude fair weather cirrus, values of $C_1 = 6$ and $C_2 = 0.5$ are generally accepted. Figure 3-3 is a spectrum of number density versus spherical radius using the Deirmendjian distribution formula. The cirrus cloud is assumed to have a density of 0.0125 gm/m^2 with mode radius 20 μm. The total number density is computed at 0.056/cc. It is shown that 70% of the particles have radii greater than 20 μm. The extinction coefficient of this distribution is equivalent to that of a monodisperse distribution of the same number density with a radius of 35 μm.

Based on the preceding arguments, an ensemble of cirrus particles of both cylinders and spheres (a coagulation of crystals or smaller cylinders) can be assumed to have a Deirmendjian type of size distribution. In such an ensemble, the optical properties of cylinders will dominate. It is then assumed that the values for 100 μm/10 μm particles can be used to represent an ensemble of particles with 50% of them greater than 80 μm, the critical size which will be hazardous to the RV transition.

The single scattering albedo and the asymmetry factor depend on the distribution and physical properties of the cloud particles. The total optical depth of the cirrus layer, on the other hand, is proportional to the product of the number density and layer thickness. For example,

TABLE 2

OPTICAL PROPERTIES OF CIRRUS AT WAVELENGTHS
0.7 μm AND 6.7 μm
(Ice crystals of 100 μm/10 μm in size with a
monodisperse distribution of 0.05 cm^{-3} is assumed.)

λ(μm)	$\gamma_{ext}(km^{-1})$	$\tilde{\omega}_o$	g
0.7	0.329	1.0	0.8
6.7	0.690	0.5	0.8

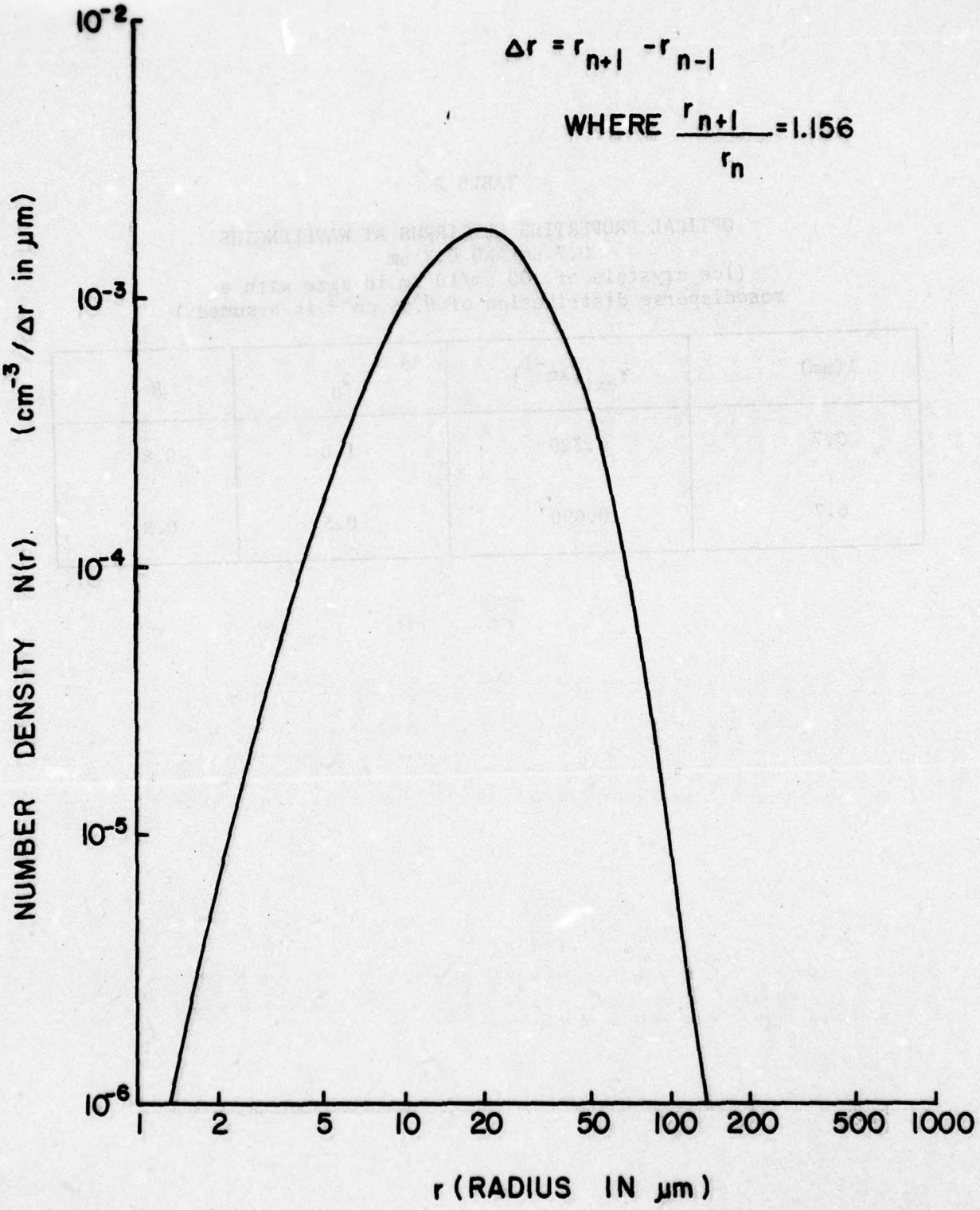

Figure 3-3 Deirmendjian size distribution of particles with mode radius of 20 μm (C_1 = 6, C_2 = 0.5, density = 0.0125 gm/m^3).

10^4 m^{-3} concentration of a 1 km path is equivalent to 5 x 10^3 m^{-3} concentration for a 2 km layer or 2 x 10^4 m^{-3} for a 1/2 km layer if the ambient atmospheric conditions in the region of cloud insertion do not vary much.

A cirrus cloud layer of 1 km (from 13 km to 14 km) is used for model computation. Once the cirrus properties are defined, they are combined with the background atmosphere to obtain a new profile of atmospheric opacity and single scattering albedo at all altitudes.

The optical properties of a cloudless atmosphere are obtained from a modified version of LOWTRAN 3B, a program developed at AFGL by Selby et al. (1976). This program has been modified at ERT such that it provides information on the atmospheric opacity and single scattering albedo at all altitudes.

Basically, LOWTRAN 3B provides a prediction of the vertical or horizontal transmittances of the atmosphere over a broad spectral range (0.25 to 28.5 μm or 350 to 40000 cm^{-1}) with resolution capability of 20 cm^{-1}. Contributions of atmospheric transmittance include the absorption of water vapor, uniformly mixed gases, ozone, nitrogen (∿4 μm), and water vapor continuum (∿10 μm), as well as molecular scattering and extinction and scattering for different aerosol models. In each case, the abundances of each species at all levels are provided; the absorption, scattering or extinction coefficient is computed for each species at different spectral regions. The uniformly mixed gases include CO_2, N_2O, CH_4, CO and O_2. The mixing ratio of these gases remains constant at all levels. The aerosol number density at each altitude for any given visual range can be prescribed as an input parameter. In addition, the solar zenith angle, is also included. Furthermore, the program provides six different types of atmospheres to choose from - tropical, mid-latitude summer, mid-latitude winter, subarctic summer, subarctic winter, 1962 standard atmosphere and a user-prescribed atmosphere.

A visibility of 23 km is selected as a clear, low haze atmosphere. The tropical atmosphere is used to represent Kwajalein environment. The combined information, together with the choice of observer angle and background reflectivity will then go through the radiative transfer model to perform multiple scattering computations.

Tables 3 and 4 are sample atmospheric profiles of optical depth and single scattering albedo at 0.7 μm. Table 3 is a case of clear

TABLE 3

OPTICAL PROFILE OF A CLEAR ATMOSPHERE
WITH VISUAL RANGE OF 23 km AT 0.7 μm

Altitude (km)	Optical Depth	Single Scattering Albedo
0.0	0.247E 00	0.806E 00
1.0	0.149E 00	0.817E 00
2.0	0.105E 00	0.837E 00
3.0	0.841E-01	0.862E 00
4.0	0.732E-01	0.869E 00
5.0	0.654E-01	0.893E 00
6.0	0.594E-01	0.915E 00
7.0	0.545E-01	0.927E 00
8.0	0.498E-01	0.931E 00
9.0	0.455E-01	0.928E 00
10.0	0.414E-01	0.921E 00
11.0	0.375E-01	0.909E 00
12.0	0.338E-01	0.900E 00
13.0	0.303E-01	0.892E 00
14.0	0.270E-01	0.881E 00
15.0	0.239E-01	0.868E 00
16.0	0.209E-01	0.851E 00
17.0	0.181E-01	0.831E 00
18.0	0.154E-01	0.806E 00
19.0	0.130E-01	0.768E 00
20.0	0.109E-01	0.719E 00
21.0	0.926E-02	0.669E 00
22.0	0.790E-02	0.620E 00
23.0	0.675E-02	0.581E 00
24.0	0.577E-02	0.551E 00
25.0	0.492E-02	0.485E 00
30.0	0.217E-02	0.372E 00
35.0	0.916E-03	0.306E 00
40.0	0.356E-03	0.310E 00
45.0	0.131E-03	0.406E 00
50.0	0.530E-04	0.593E 00
70.0	0.185E-05	0.100E 01

TABLE 4

OPTICAL PROFILE OF THE SAME ATMOSPHERE AS TABLE 3 WITH A CIRRUS LAYER ADDED BETWEEN 13-14 km (concentration of 10^4 m^{-3} of particles > 80 μm)

Altitude (km)	Optical Depth	Single Scattering Albedo
0.0	0.260E 00	0.806E 00
1.0	0.162E 00	0.817E 00
2.0	0.118E 00	0.857E 00
3.0	0.973E-01	0.862E 00
4.0	0.864E-01	0.869E 00
5.0	0.786E-01	0.893E 00
6.0	0.726E-01	0.915E 00
7.0	0.677E-01	0.927E 00
8.0	0.630E-01	0.931E 00
9.0	0.587E-01	0.928E 00
10.0	0.546E-01	0.921E 00
11.0	0.507E-01	0.909E 00
12.0	0.470E-01	0.900E 00
13.0	0.435E-01	0.978E 00
14.0	0.270E-01	0.881E 00
15.0	0.239E-01	0.868E 00
16.0	0.209E-01	0.851E 00
17.0	0.181E-01	0.831E 00
18.0	0.154E-01	0.806E 00
19.0	0.130E-01	0.768E 00
20.0	0.109E-01	0.719E 00
21.0	0.926E-02	0.669E 00
22.0	0.790E-02	.620E 00
23.0	0.675E-02	0.581E 00
24.0	0.577E-02	0.551E 00
25.0	0.492E-02	0.485E 00
30.0	0.217E-02	0.372E 00
35.0	0.916E-03	0.306E 00
40.0	0.356E-03	0.310E 00
45.0	0.131E-03	0.406E 00
50.0	0.530E-04	0.593E 00
70.0	0.185E-05	0.100E 01

atmosphere with a visibility (visual range) of 23 km. Table 4 is the same atmosphere with a 1 km cirrus layer (13 km - 14 km) with a concentration of 10^4 m^{-3} of particles greater than 80 μm. The total optical depth in a clear atmosphere is 0.247, which is equivalent to a transmittance of $e^{-0.247} = 0.78$ at the surface. The total optical depth with the insertion of the cirrus cloud is 0.260; equivalent to a reduced transmittance of $e^{-0.260} = 0.77$ at the surface. The single scattering albedo in the 13-14 km range is changed from 0.892 to 0.978 indicating a layer of more scattering effect. Both changes in the optical depth and single scattering albedo will affect the radiances at surface or in space. The computations of such changes are carried out in Section 4.

4. DETECTABILITY OF THIN CIRRUS LAYERS BY REMOTE SENSING TECHNIQUES

Theoretical estimates to predict the minimum detectable number density of ice crystals for various remote sensors are carried out in this section. The standard tropical atmosphere with a visual range of 23 km is used as ambient conditions to simulate Kwajalein atmosphere. The various remote sensors include (1) eyeball detection at the surface, (2) eyeball detection from an aircraft altitude (8-10 km), and (3) infrared (6.7 μm) sensor from space. A 20% surface reflectivity is assumed for the visual range. In the infrared region, the surface is assumed to be a perfect emitter. The optical properties of ice crystals derived from Section 3 are used as input conditions for the radiative transfer computations.

4.1 Eyeball Detection at Surface

Visual detection from the ground is the most direct and unbiased way of detecting tenuous cirrus in the reentry path. The computation of irradiances from cirrus clouds as compared to clear sky in the visible spectral range provides a means of estimating the detectibility of such cirrus by naked eyes.

Figures 4-1 to 4-4 are results of relative intensities with respect to clear atmosphere versus various concentrations of cirrus particles larger than 80 μm. A 1 km (13 km - 14 km) thick cirrus layer is assumed. Results of a 500 m layer are also presented assuming that the ambient conditions do not vary within the 13-14 km region. A minimum contrast of 10% (i.e., 10% brighter or darker than clear sky) is assumed as required for detecting the existence of cirrus visually. Figure 4-1 demonstrates results of the case when the solar zenith angle ($\cos^{-1} \mu_o$) is 0° and the look angle from zenith ($\cos^{-1} \mu$) is 37°. A minimum concentration of 1.5×10^4 m^{-3} (1 km layer) is required to give the contrast change of 10%. Figure 4-2 is the result of the case with the same look angle and the solar zenith angle of 53° indicating a slant sun; in this case a minimum concentration of 1.8×10^4 m^{-3} is required. Figures 4-3 and 4-4 are results of the cases with look angle of 66° from the zenith or 24° from the horizon. Solar zenith angles of 0° and 53° are assumed, respectively.

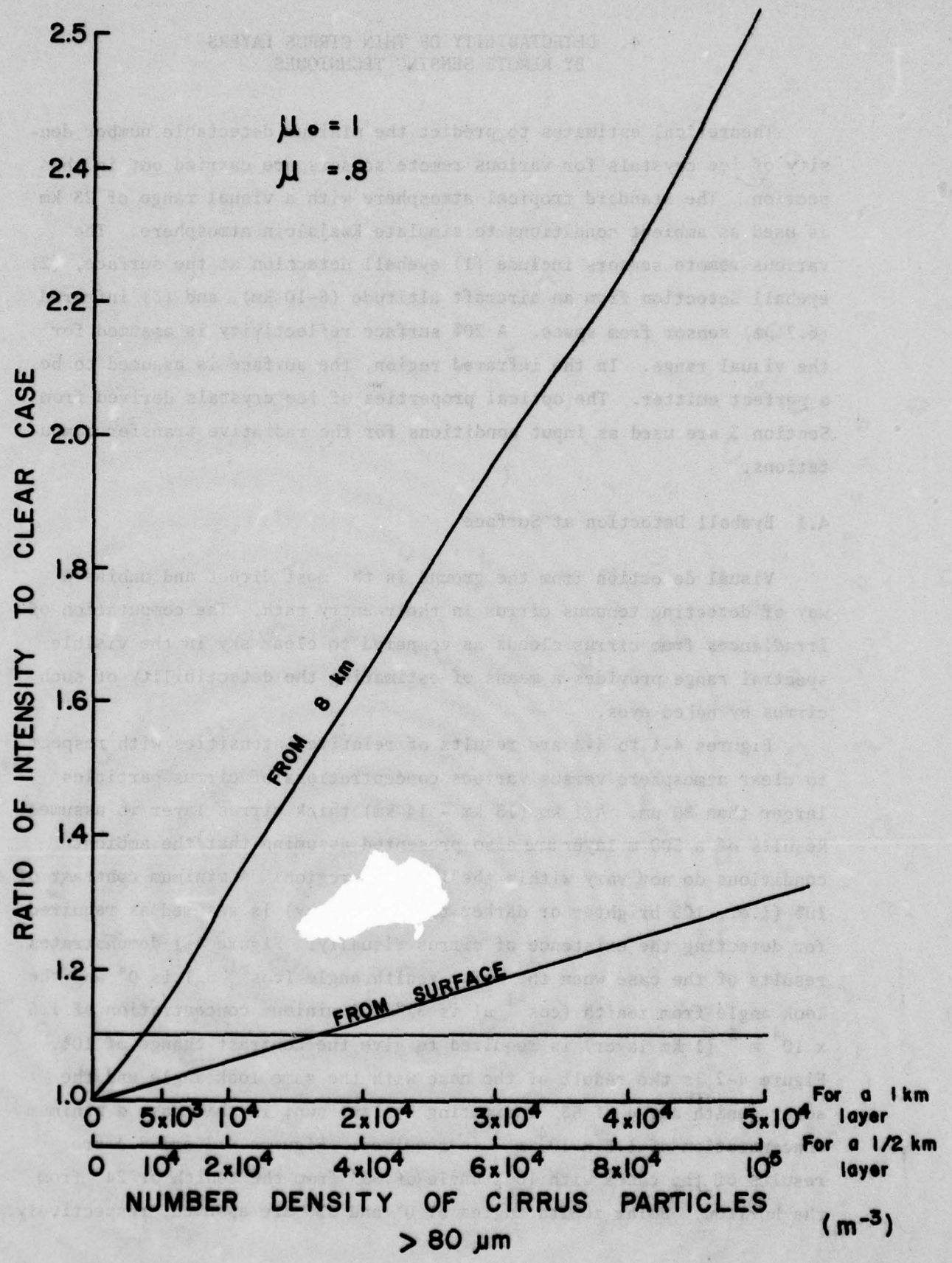

Figure 4-1 Ratio of intensity to clear case in the presence of cirrus layers at λ = 0.7 μm, μ_o = 1, μ = 0.8.

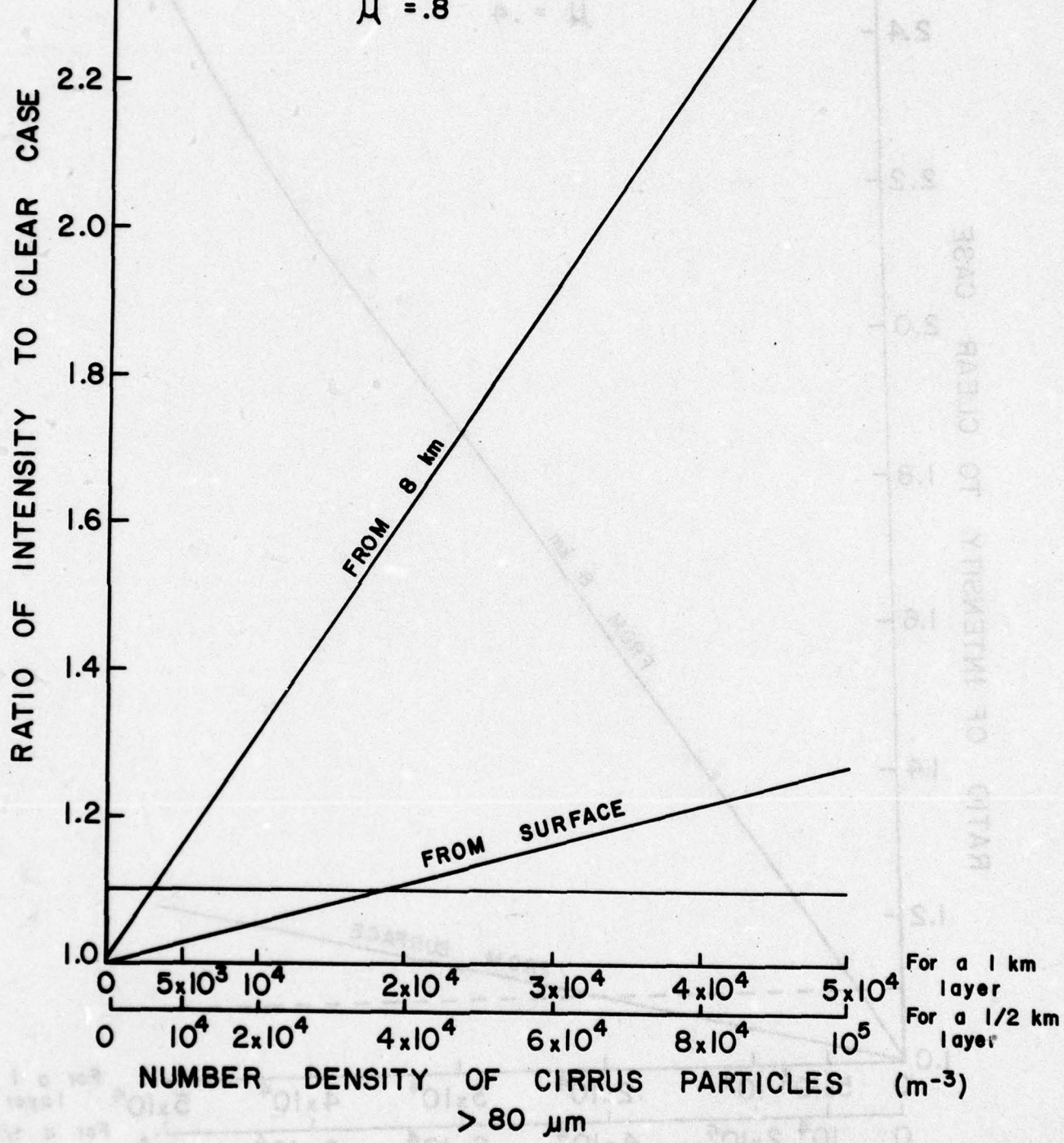

Figure 4-2 Ratio of intensity to clear case in the presence of cirrus layers at $\lambda = 0.7$ μm, $\mu_o = 0.6$, $\mu = 0.8$.

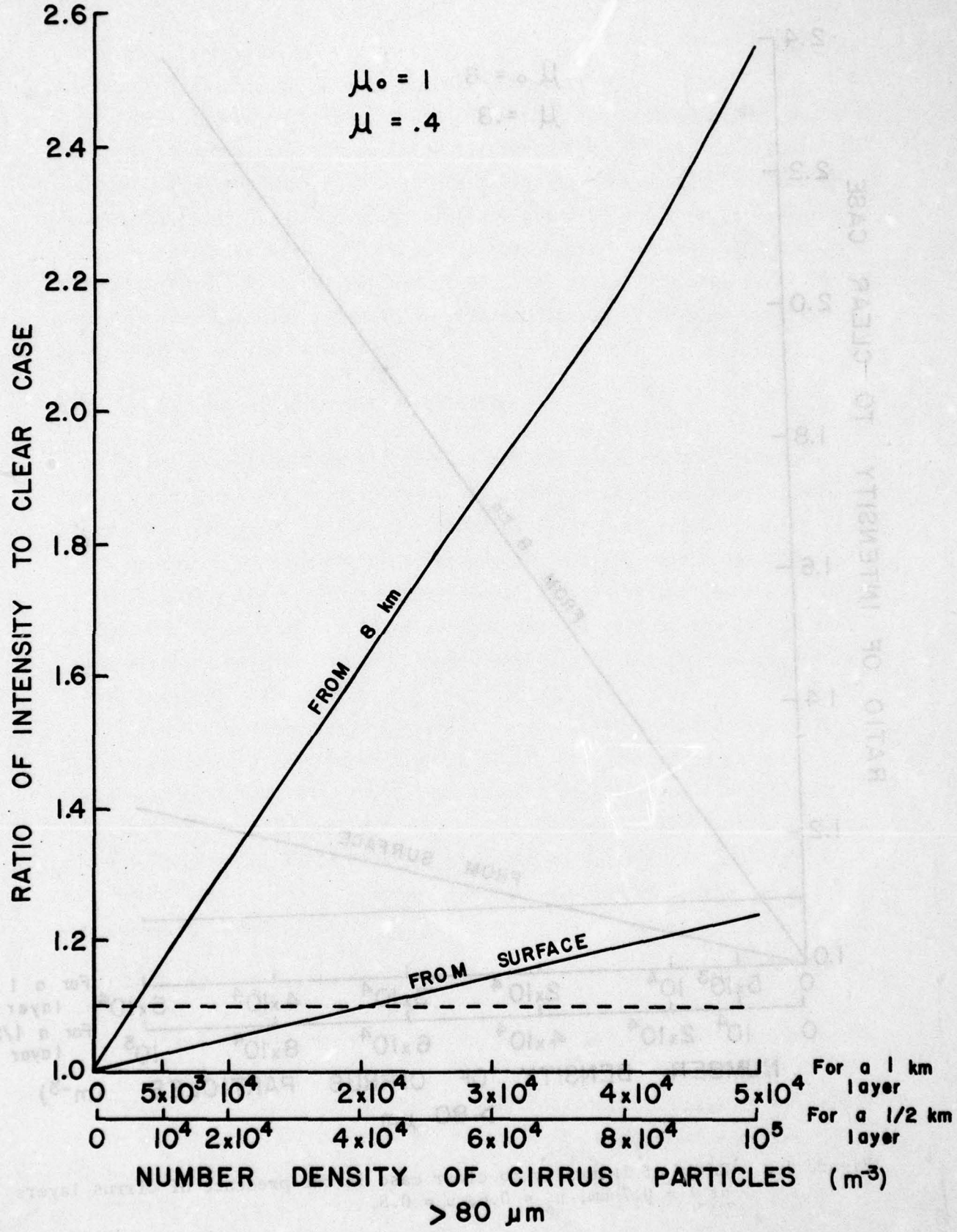

Figure 4-3 Ratio of intensity to clear case in the presence of cirrus layers at $\lambda = 0.7$ μm, $\mu_o = 1$, $\mu = 0.4$.

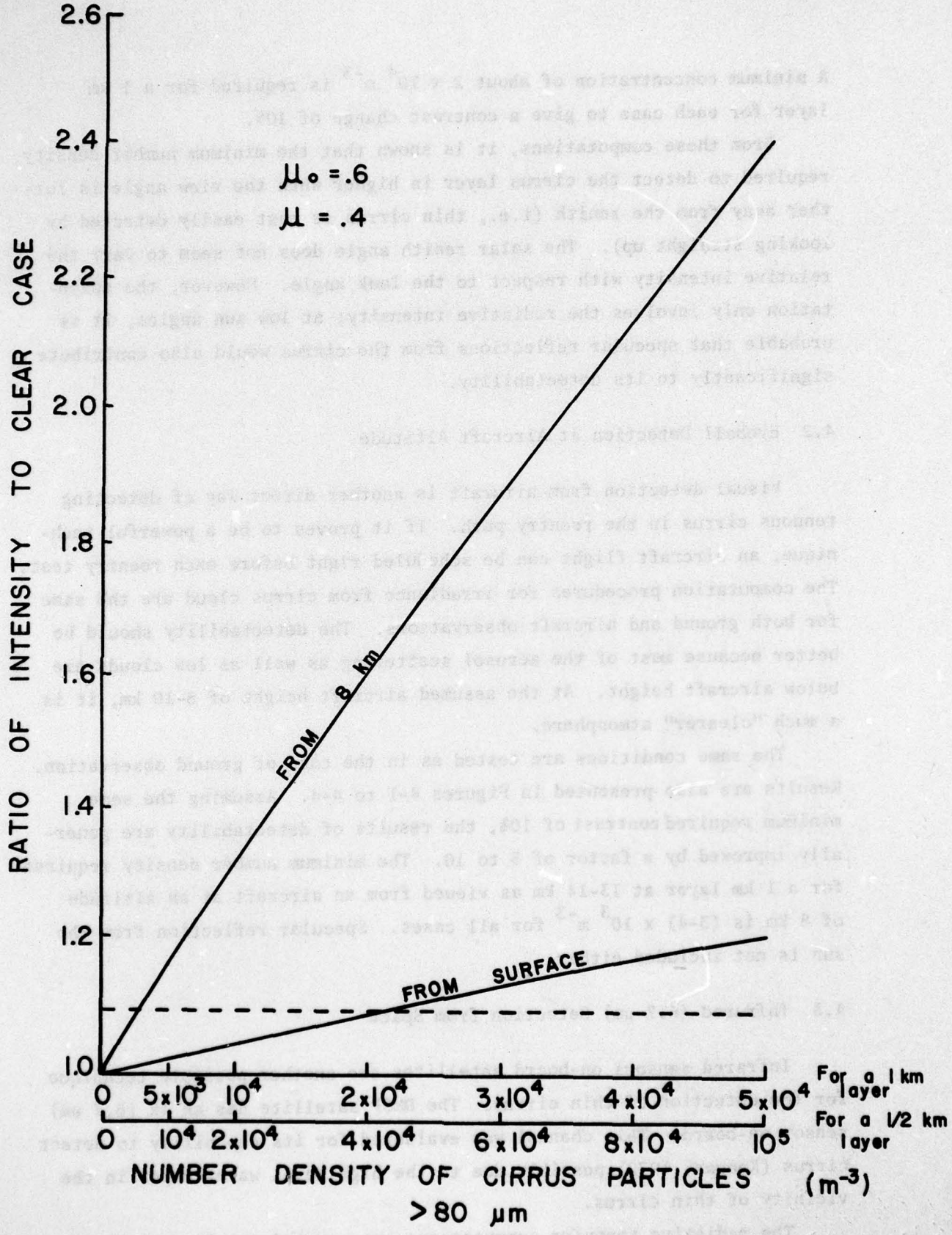

Figure 4-4 Ratio of intensity to clear case in the presence of cirrus layers at $\lambda = 0.7$ μm, $\mu_o = 0.6$, $\mu = 0.4$.

A minimum concentration of about 2 x 10^4 m^{-3} is required for a 1 km layer for each case to give a contrast change of 10%.

From these computations, it is shown that the minimum number density required to detect the cirrus layer is higher when the view angle is further away from the zenith (i.e., thin cirrus is most easily detected by looking straight up). The solar zenith angle does not seem to vary the relative intensity with respect to the look angle. However, the computation only involves the radiative intensity; at low sun angles, it is probable that specular reflections from the cirrus would also contribute significantly to its detectability.

4.2 Eyeball Detection at Aircraft Altitude

Visual detection from aircraft is another direct way of detecting tenuous cirrus in the reentry path. If it proves to be a powerful technique, an aircraft flight can be scheduled right before each reentry test. The computation procedures for irradiance from cirrus cloud are the same for both ground and aircraft observations. The detectability should be better because most of the aerosol scattering as well as low clouds are below aircraft height. At the assumed aircraft height of 8-10 km, it is a much "clearer" atmosphere.

The same conditions are tested as in the case of ground observation. Results are also presented in Figures 4-1 to 4-4. Assuming the same minimum required contrast of 10%, the results of detectability are generally improved by a factor of 5 to 10. The minimum number density required for a 1 km layer at 13-14 km as viewed from an aircraft at an altitude of 8 km is (3-4) x 10^3 m^{-3} for all cases. Specular reflection from the sun is not included either.

4.3 Infrared (6.7 μm) Detection from Space

Infrared sensors on-board satellites are another possible technique for the detection of thin cirrus. The DMSP satellite has an IR (6.7 μm) sensor on-board. This channel was evaluated for its capability to detect cirrus (Keegan, 1972) possibly due to the high level water vapor in the vicinity of thin cirrus.

The radiative transfer computations are carried out in a similar manner as in the visible spectral range. The differences are (a) the

source function comes from the atmospheric thermal emission instead of solar radiation, and (b) the intensity is converted to "brightness temperature" such that the sensitivity is defined by a fixed change in the brightness temperature instead of a percentage change relative to clear case.

A 1.5°K change from the clear case in the brightness temperature is assumed to be the minimum contrast required for detecting thin cirrus. Figure 4-5 is the results of change in brightness temperature versus various cirrus concentrations at different viewing angles. For a straight down looking ($\mu = 1.0$) sensor, the minimum required number density for a 1 km layer is approximately 5×10^3 m^{-3}. (Note the different abscissa scale of Figure 4-5 compared to Figures 4-1 to 4-4.) For a sensor look angle of 37° from vertical ($\mu = 0.8$), the required number density is reduced to 4×10^3 m^{-3}. For angles greater than 50°, the required number density is further reduced to $2\text{-}3 \times 10^3$ m^{-3}. In short, the infrared sensor has similar sensitivities as aircraft observations. The minimum number density required for an infrared sensor in space to detect thin cirrus decreases as the look angle from the vertical increases. However, as the spatial resolution will be degraded when the look angle deviates away from the vertical, changing sensor look angle away from the vertical may not be a good recommendation for improving sensor detectability.

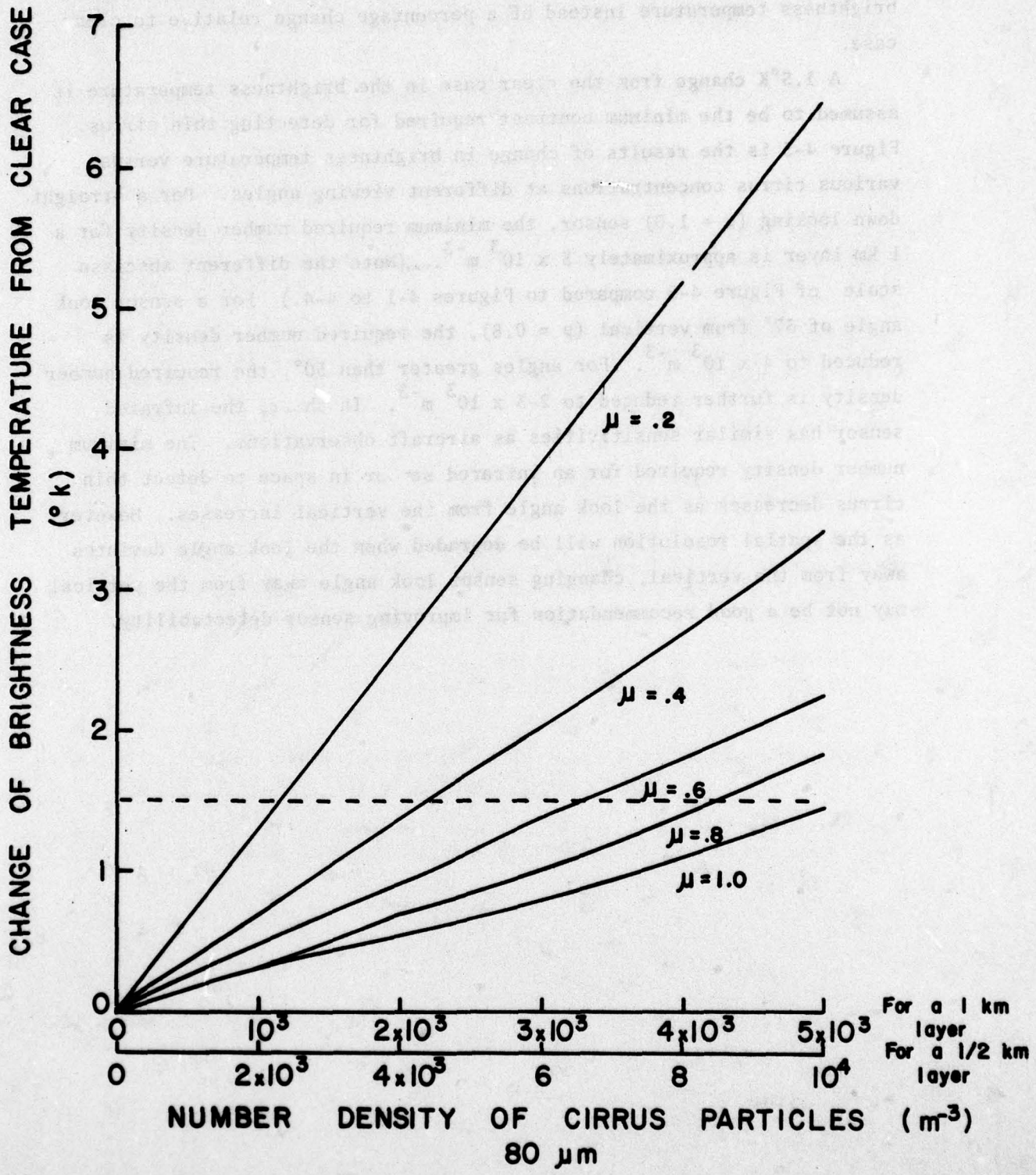

Figure 4-5 Change of brightness temperature from clear case in the presence of cirrus layers observed from space at 6.7 μm.

5. CONCLUSIONS

From theoretical computations it has been shown that thin cirrus cloud detected from aircraft observations or infrared sensors on-board satellites can be invisible from the ground. However, the required concentration of less than 1 m^{-3} of ice particles greater than 80 μm is too low a threshold (by a factor of 10^3) for virtually all the existing sensors. The probability study (Appendix C) provides a statistical review of the severe clear cases. Such severe clear cases are not established from the threshold of 1 m^{-3} of particles greater than 80 μm but from observations of cirrus combined with various meteorological criteria. This study will still be useful if the requirement for severe clear is relaxed or better sensors are developed in the future. The radiative transfer model and computer codes developed for this study will still be valid and the results (e.g. Figures 4-1 to 4-5) can still be used.

6. REFERENCES

Burke, H.K. and N.D. Sze, 1977: A Comparison of Variational and Direct Ordinate Methods for Solving Radiative Transfer Problems, J. Quart. Spectrosc. Radiat. Transfer, 17, 783.

Chandrasekhar, S., 1960: Radiative Transfer, Dover Publications, Inc., New York.

Dave, J.V., 1968: Stokes Parameters of the Radiation Scattered by a Homogeneous Sphere, 360D-17.4.002, IBM Corporation.

Gaut, N.E. and E.C. Reifenstein, III, 1969: Determination of Atmospheric and Cloud Properties from Analysis of Convair 990 Data, ERT Final Report P-002.

Van de Hulst, H.C. and K. Grossman, 1968: Multiple Light Scattering in Planetary Atmospheres, The Atmosphere of Mars and Venus, J.C. Brandt and M.B. McElroy (ed.), Gordon and Beach Publishers.

Keegan, T.J., 1972: An Evaluation of Direct Readout Infrared Data, Mon. Wea. Report, 100, 117.

Platt, C.M.R., 1973: Lidar and Radiometric Observations of Cirrus Clouds, J. Atmos. Sci., 30, 1191.

Roewe, D. and K.N. Liou, 1978: Influence of Cirrus Clouds on the Infrared Cooling Rate in the Troposphere and Lower Stratosphere, J. App. Meteor., 17, 92.

Selby, J.E.A., E.P. Shettle and R.A. McClatchey, 1976: Atmospheric Transmittance from 0.25 to 28.5 μm: Supplement LOWTRAN 3B, AFGL-TR-76-0258.

Sze, N.D., 1976: Variational Methods in Radiative Transfer Problems, J. Quart. Spectrosc. Radiat. Transfer, 16, 763.

Uthe, E.E., R.J. Allen and P.B. Russell, 1974: Light Detection and Ranging for STM-8W and PVM5 Reentry Operations, Stanford Research Institute.

APPENDIX A

SOME CHARACTERISTICS OF RADAR SYSTEMS AT KWAJALEIN

The purpose of this appendix is to compare the detection capabilities of some of the radar systems at Kwajalein. The sensitivity to detecting cirrus cloud is given by the value of the radar reflectivity factor (Z). The sensitivity to scattering from clear air refractivity index variability is given by the value of the structure constant (C_n^2). The reflectivity factor and C_n^2 are related by:

$$Z = \frac{0.378\ (C_n^2 \times 10^{18})\ \lambda^{11/3}}{\pi^5 |K|^2} \quad (mm^6\ m^{-3})$$

where λ is the radar wavelength in meters, C_n^2 in $m^{-2/3}$, and $|K|^2$ for ice particles is 0.209.

Table A-1 provides the minimum detectable values of Z for ice particles and C_n^2 at a range of 40 km for three of the radar systems at Kwajalein. Also included in the right column of the table is the concentration (in m^{-3}) of ice particles having an equivalent melted radius of 35 μm which would be needed to give the corresponding Z value. The concentrations of particles of 35 μm radius detected by the most sensitive of the radars is about double the concentrations of ice particles which might be seen visually from aircraft (see Section 4).

TABLE A-1
MINIMUM DETECTABLE Z AND C_n^2 AT A RANGE OF 40 km
FOR SOME RADAR SYSTEMS AT KWAJALEIN

Radar	λ(m)	C_n^2 ($m^{-2/3}$)	Z(mm^6/m^3)	N (m^{-3} for 70 μm diameter particles)
ALTAIR				
VCWL	1.9	4.5×10^{-18}	2.80×10^{-1}	2.3×10^{6}
UA	0.72	2.3×10^{-17}	4.08×10^{-2}	3.4×10^{5}
TRADEX				
L-CHIRP	0.2271	4.6×10^{-16}	1.10×10^{-2}	1.0×10^{5}
S-NB	0.1016	2.9×10^{-14}	3.91×10^{-2}	3.2×10^{5}
ALCOR				
C-NB	0.0529	6.4×10^{-15}	7.89×10^{-4}	6.6×10^{3}

APPENDIX B

DETECTABILITY OF THIN CIRRUS FROM LIDAR

Lidar (laser radar) provides a new indirect sensor that has unique properties for providing quantitative information on the micro- and macro-structures of cirrus clouds along the reentry path. It provides more direct information than most other remote sensors on cloud structure (height, thickness and horizontal extent), cloud phase (water droplet or ice crystal) and relative density. Realistic estimates of ice water content, crystal size and concentrations can then be carried out.

A summary of the theoretical aspect of the lidar technology was presented by Uthes, Allen and Russell (1974). The signal output can be related to atmospheric and lidar terms by the expression

$$P(R) = KER^{-2}\beta(R)\ \exp\left(\int_0^R \sigma(R)dr\right)$$

where P = received power,

E = transmitted pulse energy,

R = range from lidar,

K = lidar calibration constant,

β = volume backscatter coefficient, and

σ = volume extinction coefficient.

When dealing with tenuous cirrus, the cloud attenuation can be neglected. The cloud ice crystal number density can be estimated from

$$N_c = (P_c/P_a)(\beta_a/C_c)$$

where P_c/P_a is determined from the lidar signature, β_a is given by a least-square fit of the clear-air backscatter coefficient as a function of height Z. For the Mark IX, SRI lidar, the following relationship holds:

$$\beta_a = 6.64 \times 10^{-4}\ \exp(-0.102\ Z)\,km^{-1}sr^{-1}$$

C_c is the average cirrus particle backscatter cross section and is estimated as

$$C_c = 2\pi\ k\ a_e^{\ 2}$$

where k is the ratio of cloud backscatter to extinction coefficient and a_e is the effective spherical radius of the ice crystals defined in terms of the light.

Because of the logarithmic scale on lidar receiver, a (P_c/P_a) value of 2 (3 dB) for minimum detectable cirrus is assumed. The value $k = 0.25/4\pi$ was taken from Platt (1973). It is estimated that at a range of 15 km, a minimum number density of 5×10^3 m^{-3} is required for lidar detection assuming an effective spherical radius of 20 microns for the ice crystals.

APPENDIX C

THE PROBABILITY OF CIRRUS CLOUDS AT KWAJALEIN

The attempt of establishing a probability study of severe-clear events over Kwajalein is based primarily on routine weather observations. Surface weather observations, upper-air soundings, DMSP satellite images and RAOB reports were used to construct the original cross-section analysis of Kwajalein for the calendar year 1975 (except five days in January when radiosonde information was not available). Information from these data sources was used to determine when "severe-clear" conditions existed. Each day was divided into eight events or eight 3-hour segments. If an event had a report of no cirrus clouds visible from the surface or if it was determined that it was unlikely that cirrus clouds extended above the 10 km level then it would be investigated further to determine whether this was a severe-clear or tenuous cirrus case. The event was labeled tenuous cirrus if the event immediately before or after it had a surface report of cirrus clouds thus establishing a sort of "buffer zone" requirement for clearing the atmosphere of lingering crystals after or before the passage of a cirrus cloud. Furthermore, if there was substantial convective activity in the Kwajalein area during an event, the event was labeled as tenuous cirrus. A case was determined to be severe-clear when it had passed the buffer zone requirement, there was no convective activity reported and the upper atmosphere (10 to 17 km level) was dry (dew point depressions of 10°C or more).

It is usually assumed that the highest probability of having severe-clear conditions at Kwajalein will occur during the winter months of December through February. Figure C-1 shows the probability in percent of having no cirrus reported as determined from surface observations and an assessment of the dew point depressions above a height of 10 km. Using the criteria of tenuous cirrus and severe clear as defined in the previous paragraph the percent probabilities of these events are also shown in Figure C-1. Note that the probability of having a severe-clear atmosphere in March of 1975 was 27.4%; in December it was 12.5%, and in February it was 10.7%. However, in January, even though there was relatively little convective activity, there was no severe-clear case or even a no cirrus event as defined above (five days in January were not

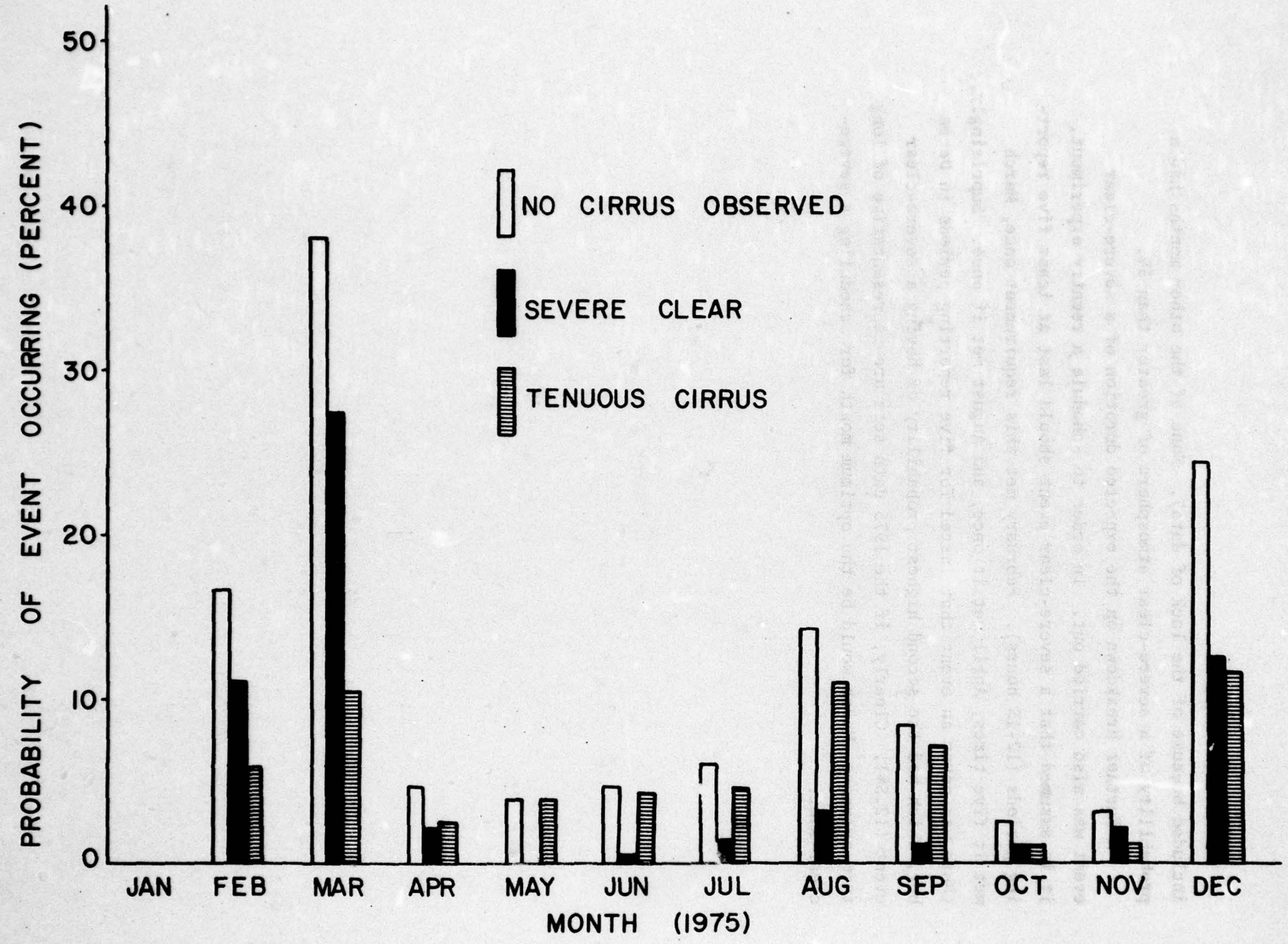

Figure C-1. The probabilities of having no cirrus, tenuous cirrus and severe-clear for each month of 1975 at Kwajalein. The categories of cirrus conditions are defined in the text.

included because of the lack of data). None of the other months had a probability of a severe-clear atmosphere of greater than 5%.

A further breakdown on the expected duration of a severe-clear event was also carried out. In order to schedule a reentry experiment, it is assumed that a severe-clear event should last at least five reporting periods (12-15 hours). February met this requirement once, March met it five times, April met it once, and August met it once. Suprisingly, there was never an event that lasted for five reporting periods in December, which had the second highest probability of having a severe-clear event (12.5%). Clearly, if the 1975 data sets are representative of long term averages, March would be the optimum month for scheduling a severe-clear shot.

APPENDIX D

THE VARIATIONAL-ITERATIVE TECHNIQUE FOR SOLVING RADIATIVE TRANSFER EQUATION

The source function of the radiative transfer equation described in Section 2 can be rewritten as

$$J(\tau) = J_o(\tau) + \frac{\omega_o(\tau)}{2} \int_o^{\tau^*} J(t)E_1(|t-\tau|)dt$$
$$+ \frac{\omega_o(\tau)}{2} \cdot E_2(\tau^*-\tau)[(1-R)B(T_{gr}) + 2 \cdot R \cdot \int_o^{\tau^*} J(t)E_2(\tau^*-t)dt] \quad \text{(D-1)}$$

(the third term is 0 in the visible range) where the exponential integral E_n of the n^{th} order is defined as

$$E_n(x) = \int_o^1 e^{-x/\mu}\, \mu^{n-2}\, d\mu \qquad n = 1,2,\ldots$$

The variational-iterative technique was first developed by Sze (1976) and extended by Burke and Sze (1977). It provides a direct method for constructing an approximate solution to the integral equation for the source function.

The VI technique provides a direct method for constructing an approximate solution to the integral equation (D-1) for the source function. An approximate source function can be expressed as

$$J_a(\tau) = U_a(\tau)\sqrt{\omega_o(\tau)}$$

where

$$U_a(\tau) = \sum_{i=1}^{N} C_i V_i(\tau)$$

and the $V_i(\tau)$ are known trial functions. The choice of trial functions plays an important role in the ultimate success of the variational method (Kourganoff, 1963). In the variational solution, simple step functions were chosen as the trial functions. This choice (1) makes it simple to perform the integrals required in (D-1) and (2) the intervals can be chosen to resemble multiple cloud layers, the weights $C_i\sqrt{\omega_i}$ for each layer represent the average source function in that layer where ω_i is the single scattering albedo for the layer.

The total optical depth τ^* is divided into N-1 intervals with ω_i constant over each interval. The trial function then is

$$V_j(\tau) = \begin{cases} 1 & \tau_j < \tau \leq \tau_{j+1} \\ 0 & \text{otherwise} \end{cases}$$

The C_i then are solutions of the algebraic equation

$$\sum_{j=1}^{N} M_{ij} C_j = f_i$$

where $$M_{ij} = \delta_{ij}\Delta\tau_j - \sqrt{\frac{\omega_i \omega_j}{2}} \int_{\tau_i}^{\tau_{i+1}} D_j(\tau)\,dr$$

$$\delta_{ij} = \begin{cases} 0, & i \neq j \\ 1, & i = j \end{cases}$$

$$D_j(\tau) = \int_{\tau}^{\tau_{j+1}} E_1(|\tau - t|)\,dt$$

and $$f_1 = \left(\frac{1-\omega_i}{\sqrt{\omega_i}}\right) B(T(\tau_i)) + \frac{\sqrt{\omega_i}}{2} E_2(\tau^* - \tau_i)\ (1-R)B(T_s)$$

The variational solution is an approximation to the actual solution which is correct at least at one level within each layer. A smoothed approximation for the source function then can be constructed:

$$J_1(\tau) = J_o(\tau) + \frac{\omega_o(\tau)}{2} E_2(\tau^* - \tau)(1-R)B(T_s)$$

$$+ \frac{\omega_o(\tau)}{2} \sum_{j=1}^{N-1} C_j \sqrt{\omega_j(\tau)}\ D_j(\tau)$$

$$+ \omega_o(\tau)\ E_2(\tau^* - \tau)\ R \sum_{j=1}^{N-1} C_j \sqrt{\omega_j(\tau)} \int_{\tau_j}^{\tau_{j+1}} E_2(\tau^* - t)\,dt$$

Since the smoothed approximation is a summation over layers with oscillating residual errors, it provides a reasonable first estimate of the true source function. Improved accuracy may be obtained by further

iterations of the integral equation for the source function as:

$$J_{n+1}(\tau) = J_o(\tau) + \frac{\omega_o(\tau)}{2} E_2(\tau^*-\tau)(1-R)B(T_s)$$

$$+ \frac{\omega_o(\tau)}{2} \int_{\tau}^{\tau^*} E_1(|\tau-t|)J_n(t)dt$$

$$+ \omega_o(\tau)\ E_2(\tau^*-\tau)\ R \int_o^{\tau^*} E_2(\tau^*-t)J_n(t)dt$$

The residue of the nth iteration is defined as

$$\Delta_n = \left| \frac{J_n - J_{n-1}}{J_n} \right|$$

By specifying the maximum residue allowed, the iteration process then brings the source function to desired accuracy.